HEALTH AND MEDICINE

Enhanced immunocompatibility and hemocompatibility of nanomedicines across multiple species using complement pathway inhibitors

Yue Li[1]†, Sarah Jacques[1]†, Hanmant Gaikwad[1], Morgan Nebbia[1], Nirmal K. Banda[2], V. Michael Holers[2], Stephen A. Tomlinson[3,4], Robert I. Scheinman[1], Andrew Monte[1,5,6], Laura Saba[1], Erika Lasda[7], Jay Hasselberth[7], Nicolas Busquet[8], Wioleta M. Zelek[9], S. Moein Moghimi[1,10,11], Dmitri Simberg[1]*

The activation of complement by nanomedicines triggers immune uptake and proinflammatory responses. Complement pathway inhibitors could offer strategies to address these challenges. Here, we assess the efficacy of inhibitors with various nanoparticles, including dextran superparamagnetic iron oxide nanoworms, polyethylene glycol (PEG) liposomal drugs, and mRNA lipid nanoparticles. In human sera, inhibitors of the alternative pathway iptacopan and danicopan exhibit variable efficacies, ranging from high nanomolar to incomplete inhibition. However, both iptacopan and danicopan display poor efficacy with PEGylated liposomal doxorubicin. Sutimlimab, an inhibitor of the classical pathway, demonstrates poor efficacy with PEGylated liposomal doxorubicin, even in sera with anti-PEG antibodies. Iptacopan displays donor-dependent inhibition of the uptake of nanoparticles in human blood. Bolus coadministration of iptacopan with nanoworms in mice, rats, and dogs inhibits C3 opsonization and uptake by granulocytes. Iptacopan also alleviates nanoparticle-induced lethargy in rats and severe hypotension in dogs. These data suggest that complement inhibitors can enhance the immunocompatibility and hemocompatibility of nanomedicines in a donor-dependent manner.

INTRODUCTION

Nanoparticles' small size, multifunctionality, and ability to encapsulate drugs and imaging agents make them attractive for treating and diagnosing diseases such as cancer, infections, and genetic disorders. However, patients experience hypersensitivity and acute immune responses to nanoparticles, which require slower administration, premedication with drugs, including antihistamines and/or corticosteroids, and monitoring by trained health care staff (*1*).

The complement system is critical for identifying foreign nanoparticles and pathogens and clearing them from the body, but its overactivation could result in acute proinflammatory responses (*2*). The complement system (Fig. 1) is incited via three distinct pathways [classical (CP), lectin (LP), and alternative (AP)] that converge to the third component of complement C3 (*2*). C3 cleavage by classical (C4bC2a) and alternative [C3b($C3H_2O$)/Bb] convertases generates additional C3b that covalently binds to a foreign surface. C3b is proteolytically processed into iC3b, C3dg, and C3d; these species prime the surface of a nanoparticle for recognition through complement receptors [complement receptor 3 (CR3) for iC3b and CR2 for C3d] expressed on blood and tissue phagocytes, including neutrophils, monocytes, dendritic cells, and resident macrophages (*2*, *3*). This uptake decreases efficacy and contributes to proinflammatory responses toward nanomedicine (*4*, *5*). Furthermore, the liberation of C3a and C5a triggers chemotaxis, activation of inflammatory cells, and anaphylaxis, whereas the assembly of the membrane attack complex (C5b-C9) leads to cell lysis and proinflammatory pathway activation (*2*).

Among approved nanomedicines, administration of polyethylene glycol (PEGylated) liposomal doxorubicin (PLD; Doxil), iron carbohydrate complexes (Feraheme), liposomal irinotecan (Onivyde), and micellar paclitaxel (Taxol) triggers infusion reactions in some individuals (*1*). Infusion reactions have led to the suspension of advanced clinical trials or withdrawal of drugs from the market, as seen with PEGylated drugs peginesatide (Omontys), pegloticase (Krystexxa), pegnivacogin (Revolixys), and dextran iron oxide contrast agents Sinerem and Resovist (*6*–*10*). While complement inhibitors are not now approved for clinical use to prevent nanoparticle-induced hypersensitivity, complement inhibition can offer a generic, orthogonal (independent of the nanoparticle surface) method to prevent complement opsonization and improve the hemocompatibility and immunocompatibility of nanomedicines. In that regard, complement therapeutics is a rapidly evolving approach for the treatment of complement-dependent disorders (*11*, *12*). Recently, orally bioavailable small molecule inhibitors of the alternative complement pathway iptacopan (Fabhalta) and danicopan (Voydeya) have been approved by the US Food and Drug Administration (FDA) for paroxysmal nocturnal hemoglobinuria (PNH) and atypical hemolytic uremic syndrome (*13*). Iptacopan binds with

[1]Department of Pharmaceutical Sciences, The Skaggs School of Pharmacy and Pharmaceutical Sciences, University of Colorado Anschutz Medical Campus, Aurora, CO 80045, USA. [2]Division of Rheumatology, School of Medicine, University of Colorado Anschutz Medical Campus, Aurora, CO 80045, USA. [3]Department of Microbiology and Immunology, Medical University of South Carolina, Charleston, SC 92425, USA. [4]Ralph Johnson Veterans Affairs Medical Center, Charleston, SC 92425, USA. [5]Rocky Mountain Poison & Drug Safety at Denver Health & Hospital Authority, Denver, CO 80204, USA. [6]Department of Emergency Medicine, University of Colorado Anschutz Medical Campus, Aurora, CO 80045, USA. [7]University of Colorado School of Medicine, Department of Biochemistry and Molecular Genetics, RNA Bioscience Initiative, University of Colorado Anschutz Medical Campus, Aurora, CO 80045, USA. [8]NeuroTechnology Center's Animal Behavior and In Vivo Neurophysiology Core, University of Colorado Anschutz Medical Campus, Aurora, CO 80045, USA. [9]UK Dementia Research Institute Cardiff and Division of Infection and Immunity, School of Medicine, Cardiff University, Cardiff, Wales, UK. [10]School of Pharmacy, Newcastle University, Newcastle upon Tyne NE1 7RU, UK. [11]Translational and Clinical Research Institute, Faculty of Health and Medical Sciences, Newcastle University, Newcastle upon Tyne NE2 4HH, UK.
*Corresponding author. Email: dmitri.simberg@cuanschutz.edu
†These authors contributed equally to this work.

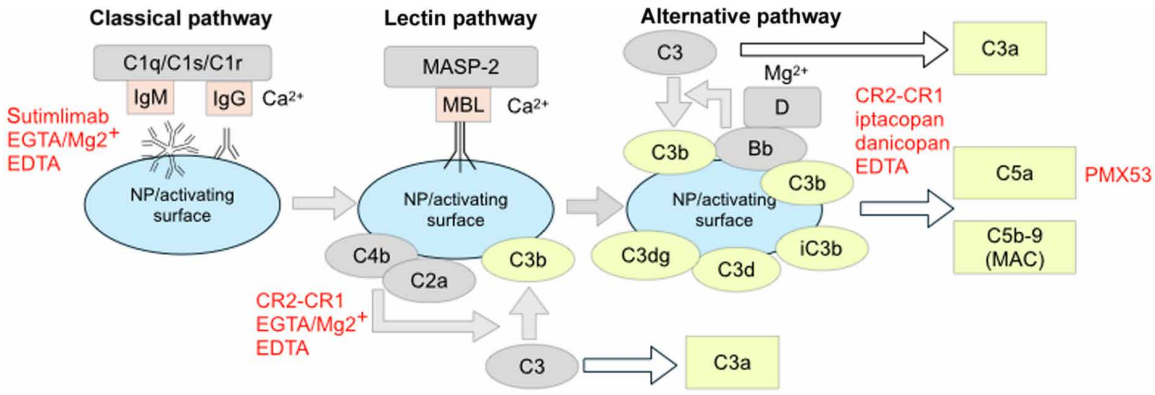

Fig. 1. Complement activation pathways. In red are the inhibitors explored in this study

nanomolar affinity to complement factor B and prevents its cleavage into Bb. Danicopan binds to complement factor D and prevents the enzymatic processing of factor B into Ba and Bb (*13*). Sutimlimab (Enjaymo) is a monoclonal antibody that has been approved for cold agglutinin disease (*14*). It binds to C1s and prevents its activation and the enzymatic conversion of C2 and C4 into classical convertase C4bC2a. The PEGylated derivative of cP40 (pegcetacoplan, Empaveli) exerts its function by binding to the entire pool of C3 and allosterically inhibiting its cleavage by convertases (*15*). Eculizumab (Soliris), a monoclonal antibody that blocks complement protein C5 and prevents the generation of C5a and C5b-C9, is also approved for PNH (*16*). Other inhibitors include potent antagonists of the C5a receptor, PMX53, and avacopan (recently approved for antineutrophil cytoplasmic antibody-associated vasculitis (*17*)). Complement regulators are another promising group of therapeutics based on natural complement inhibitors. Thus, CR2-CR1 (TT32) is the fusion of 4 domains of CR2 and 10 domains of CR1 (*18*). CR2 binds to the initial complement deposits, including iC3b and C3d. It brings to the surface CR1 that inhibits the alternative C3bBb and classical C4bC2a convertases (*19*) as well as C5 convertases and serves as a cofactor for the complement factor I for degradation of C3b to iC3b and then to C3dg (*20*). CR2-CR1 exhibits low nanomolar to high picomolar median inhibitory concentration (IC_{50}) for many types of nanoparticles (*21*).

Despite the emergence of multiple clinically approved inhibitors, their combination with nanomedicines, i.e., the inhibition of complement opsonization and immune cell uptake, has not been tested. Our results demonstrate that the inhibitor of the alternative pathway iptacopan can improve hemocompatibility, suppress immune uptake, and prevent acute reactions toward bolus-injected nanoparticles in multiple species, potentially making the drug suitable for clinical testing. While we found it to be less versatile and potent than the targeted complement regulator CR2-CR1, iptacopan may be helpful in improving the immunocompatibility and hemocompatibility of bolus injection of certain classes of nanoparticles, providing safer and more effective treatments for patients.

RESULTS

Variable, donor-dependent efficacy of the complement inhibitors in human sera and plasma

The efficacy of the AP inhibitors iptacopan, danicopan, and multipathway inhibitor CR2-CR1 (Fig. 1) was assessed in healthy donor's serum using the set of preclinical and clinical nanoparticles (table S1): superparamagnetic iron oxide nanoworms (SPIO NWs, 112 nm), cross-linked iron oxide NWs (CLIO NWs, 123 nm), FDA-approved PLD (82 nm), and FDA-approved liposomal irinotecan (Onivyde, 108 nm). C3 deposition was measured with a C3 dot-blot immunoassay (*22*). We previously demonstrated that C3 deposition measurement by the dot-blot correlates with fluid phase activation (*22*). Nevertheless, C5a in the fluid phase was also measured (Fig. 2A). Given the emerging concerns with the reactions associated with lipid nanoparticle (LNP) formulations such as FDA-approved Onpattro (*23*), as well as mRNA vaccines (*24*), we prepared mRNA LNPs using Onpattro lipid composition (114 nm). Since LNPs could not be pelleted to measure C3 deposition, we relied only on C5a measurements to determine the level of complement activation. According to Fig. 2B and Table 1, iptacopan and danicopan demonstrated low micromolar inhibitory concentration (IC_{50}) of C3 deposition on SPIO NWs, CLIO NWs, and Onivyde. Notably, for PLD, iptacopan and danicopan showed less than 50% inhibition at 100 μM. On the other hand, CR2-CR1 showed a single nanomolar IC_{50} for all the particles and almost complete inhibition of C3 deposition. We measured the C5a IC_{50} of iptacopan, danicopan, and CR2-CR1. We observed a similar trend as with C3 deposition, i.e., lower efficacy of iptacopan and danicopan than CR2-CR1 (Table 2 and fig. S1).

For mRNA LNPs, we measured C5a IC_{50} for iptacopan, danicopan, and CR2-CR1 in sera from three healthy donors (Fig. 2C and Table 2). CR2-CR1 showed single-nanomolar potency and completely inhibited C5a release at 30 nM in all three donors. Iptacopan and danicopan demonstrated low micromolar IC_{50} values and completely inhibited C5a release at 100 μM in donors F38 and M61 but resulted in less than 60% inhibition in donor F46 (Fig. 2C).

Complement activation in humans is highly variable and dictated by the subject-dependent levels of nanoparticle-binding antibodies (*25*) as well as other factors collectively referred to as "complotype" (*26*). Nanoparticle-recognizing antibodies, primarily anti–polyethylene glycol (PEG) antibodies, emerge as a concern due to their association with hypersensitivity reactions and enhanced complement activation (*27*–*29*). To understand how the inhibitors perform in donors with variable levels of anti-PEG antibodies, we used lepirudin anticoagulated plasma from 10 donors with variable levels of anti-PEG immunoglobulin G (IgG) and immunoglobulin M (IgM) [Fig. 3A and (*25*)]. In all donors, CR2-CR1 at 10 nM blocked, on average, 67% of C3 on PLD, similar to 10 mM EDTA. In contrast,

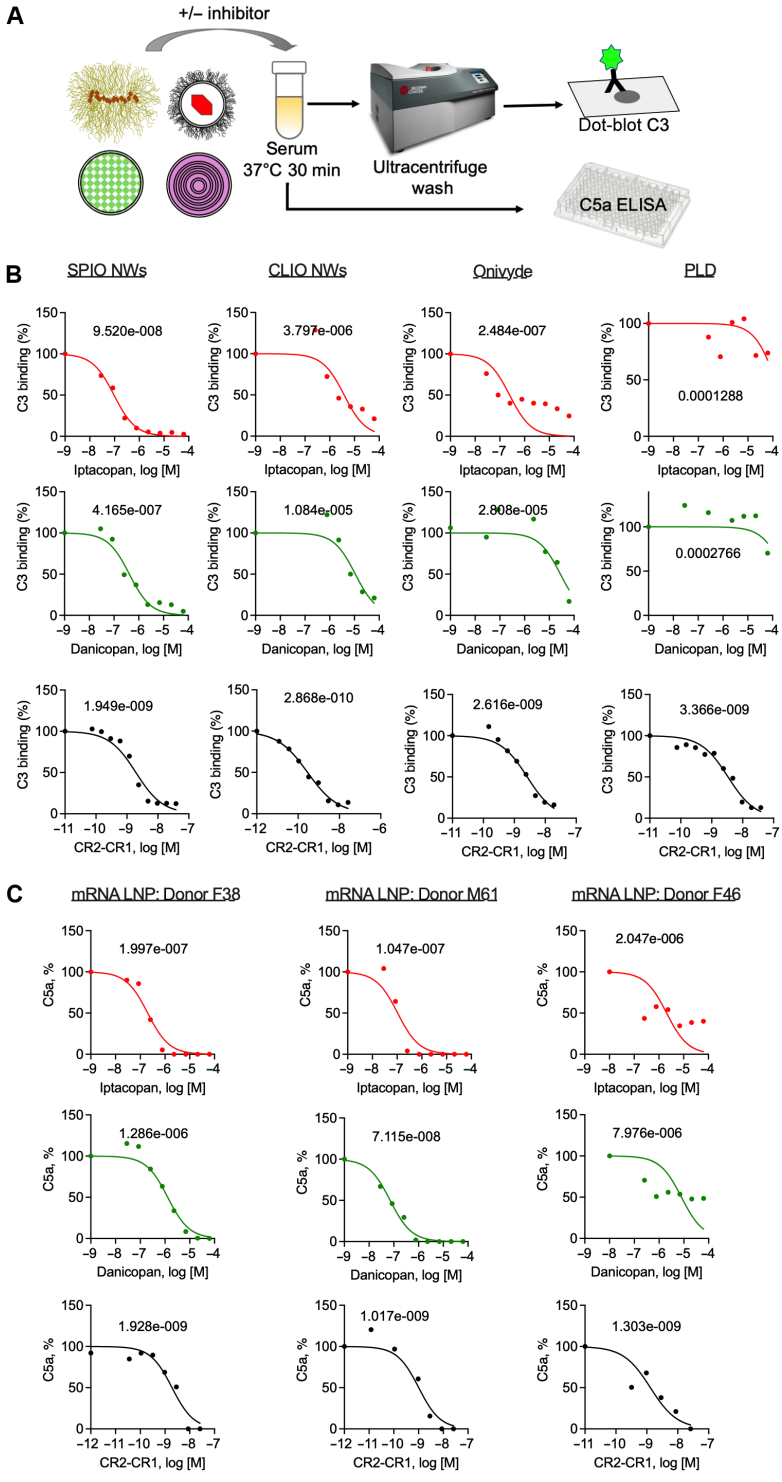

Fig. 2. Efficacy of complement inhibitors combined with different classes of nanomedicines. (**A**) Experimental workflow. Inhibitors were added at various concentrations to the serum, followed by the nanoparticles. Complement C3 deposition was quantified by a dot blot immunoassay and C5a generation by enzyme-linked immunosorbent assay (ELISA). (**B**) Inhibitory concentrations of C3 deposition. Top row: Iptacopan. Middle row: Danicopan. Bottom row: CR2-CR1. Both iptacopan and danicopan have limited efficacy with PLD. Experiments were repeated twice. (**C**) C5a IC_{50} of iptacopan, danicopan, and CR2-CR1 with mRNA LNPs in three different donors. In donor F46, iptacopan and danicopan are not as effective as in the other donors. Inhibitory curves for SPIO NWs, CLIO NWs, Onivyde, and PLD are in the supplementary figures.

Table 1. IC_{50} values for human C3 deposition.

C3, IC_{50}, molar	SPIO NWs	CLIO NWs	Onivyde	PLD
Iptacopan	9.52×10^{-008}	3.98×10^{-006}	2.48×10^{-007}	0.0001288
Danicopan	4.17×10^{-007}	1.08×10^{-005}	2.81×10^{-005}	0.0002766
CR2-CR1	1.95×10^{-009}	2.85×10^{-010}	2.6×10^{-009}	3.37×10^{-009}

Table 2. IC_{50} values for human C5a release in the fluid phase.

C5a, IC_{50}, molar	SPIO NWs	CLIO NWs	Onivyde	PLD	mRNA LNPs
Iptacopan	4.63×10^{-008}	4.77×10^{-008}	2.20×10^{-008}	3.17×10^{-007}	1.05×10^{-007} 2.05×10^{-006} 1.20×10^{-007}
Danicopan	6.97×10^{-009}	6.93×10^{-009}	2.58×10^{-006}	0.000175	7.12×10^{-008} 7.98×10^{-006} 1.29×10^{-006}
CR2-CR1	7.25×10^{-010}	1.48×10^{-09}	1.267×10^{-009}	1.166×10^{-008}	1.02×10^{-009} 1.30×10^{-009} 1.93×10^{-009}

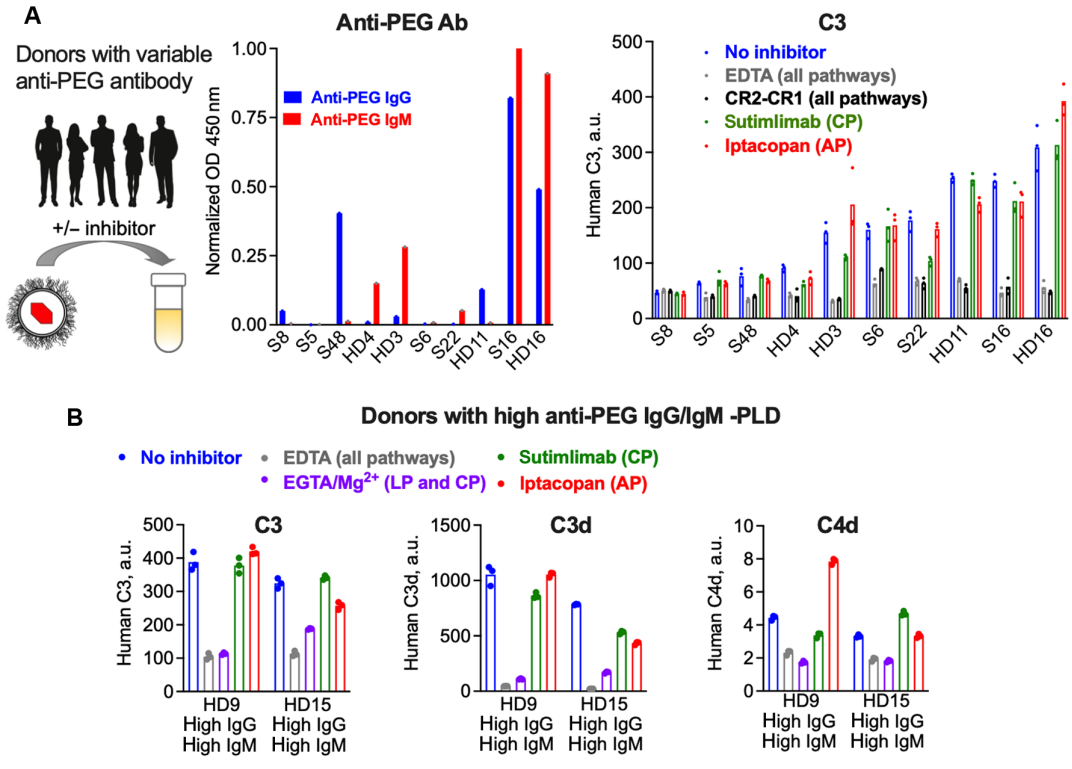

Fig. 3. Inhibition of opsonization of PLD by pathway inhibitors in donors with variable complement activation. (**A**) Left graph: Lepiridin plasma ($n = 10$, labels on the *x* axis show sex and age) with variable levels of anti-PEG IgG and IgM was used to evaluate the inhibition of C3 opsonization of PLD. Right graph: C3 deposition. Sutimlimab and iptacopan are minimally effective (EDTA, 10 mM; CR2-CR1, 10 nM; sutimlimab, 200 μg/ml; iptacopan, 10 μM). OD, optical density; Ab, antibody. (**B**) Inhibition of deposition of C3, C3d, and C4d (CP and LP) in donors with the top 10th percentile titer of anti-PEG IgG and IgM. Sutimlimab exhibits marginal effectiveness at inhibiting C3 opsonization. Iptacopan is also marginally effective. Notably, sutimlimab does not inhibit C4d deposition on PLD, suggesting the contribution of the lectin pathway (EDTA, 10 mM; EGTA/Mg^{2+}, 10 mM; sutimlimab, 200 μg/ml; iptacopan, 10 μM). Bars show the means of three technical replicates. Repeated twice. a.u., arbitrary units.

sutimlimab (CP inhibitor) at 200 μg/ml and iptacopan at 10 μM showed no inhibition of C3 deposition on PLD (Fig. 3A).

To further understand the involvement of complement pathways in donors with high levels of anti-PEG antibodies, we used plasma from two donors with high titers of anti-PEG IgG/IgM [top 10th percentile among the subjects we tested (*25*)] to measure C3, C3d, and C4d (CP and LP markers) deposition. In addition to iptacopan and sutimlimab, we tested EGTA/Mg^{2+}, which blocks both CP and LP (Fig. 1). Sutimlimab and iptacopan showed minimal inhibition of C3 opsonization of PLD (Fig. 3B). EGTA/Mg^{2+} showed strong inhibition of C3 deposition on PLD. EGTA/Mg^{2+} but not sutimlimab inhibited the opsonization of PLD with C4d, suggesting the involvement of the LP. Notably, EDTA only partially inhibited C3 opsonization of PLD. Some of the surface-bound C3 could be C3(H_2O) rather than C3b/iC3b/C3d (*30*), which could result in nonproteolytic activation of the complement and not be inhibited by EDTA. The presence of a full-size, non-inhibitable C3 was previously demonstrated for liposomes (*31*) and other nanoparticles (*32*). C3d, a specific cleavage fragment of C3 convertase, showed full inhibition with EDTA and EGTA/Mg^{2+} (Fig. 3B) but only partial activity of sutimlimab and iptacopan. Collectively, these data demonstrate that the classical or the alternative pathway alone cannot explain the C3 opsonization. The substantial between-subject variability in the pathway of activation could be the reason that inhibitors of a single pathway were less efficient than pan-C3 convertase inhibitor CR2-CR1.

Variable, donor-dependent efficacy of the complement inhibitors in preventing immune uptake in human blood

Given the critical role of complement in the immune uptake of nanoparticles by blood phagocytes (*33*, *34*), we used flow cytometry to measure the inhibitors' effect on the uptake. We used SPIO NWs and DiD-labeled mRNA LNPs, and we also prepared DiD-labeled PEGylated liposomes {PLD formula, 126 nm polydispersity index [(PDI), 0.1]}. Nanoparticles were added to the fresh lepirudin-anticoagulated blood and incubated for 1 hour at 37°C, followed by red blood cell (RBC) lysis for liposomes and mRNA LNPs or magnetic separation for SPIO NWs (Fig. 4A). First, we investigated which cell

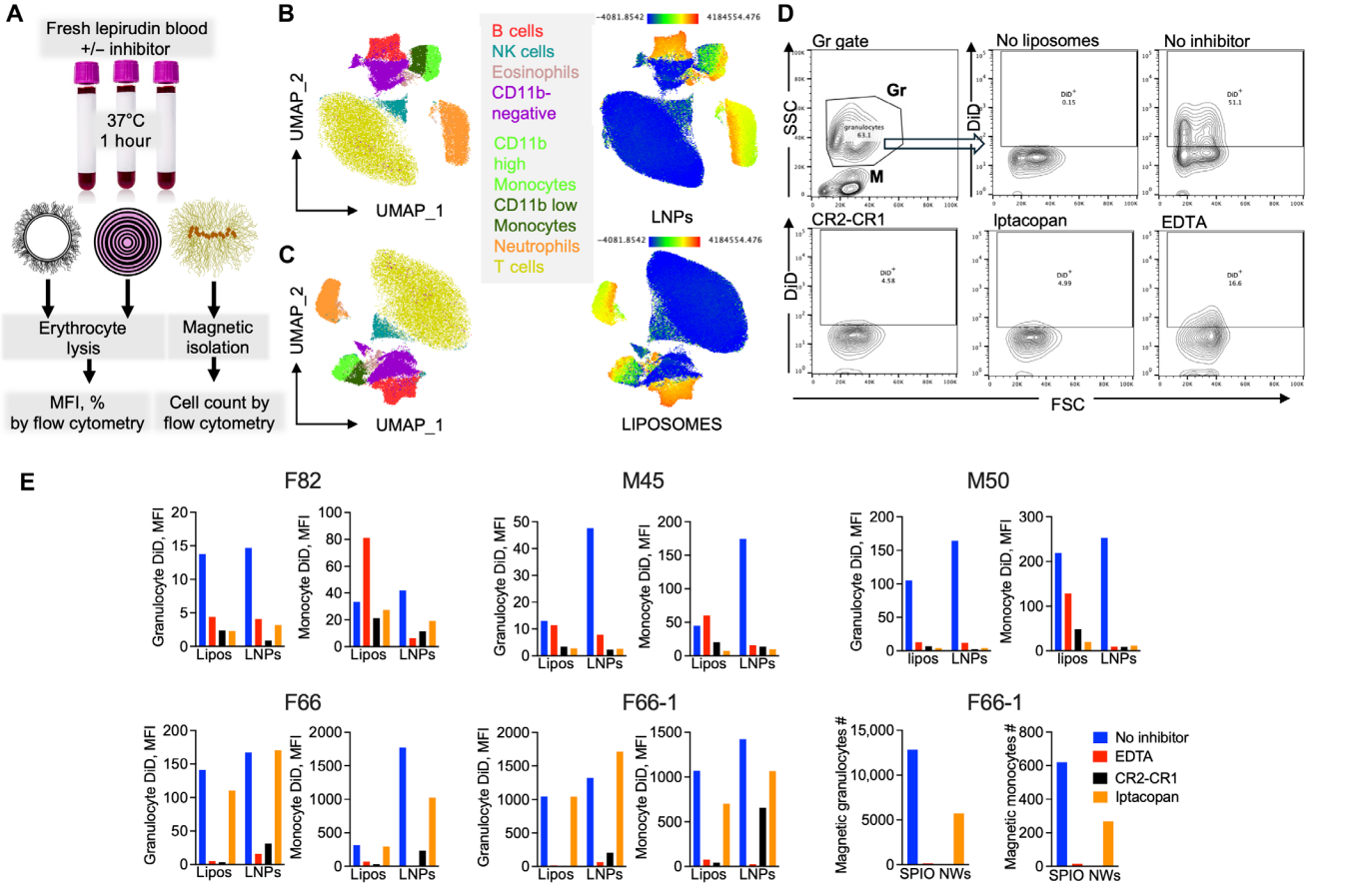

Fig. 4. Donor-dependent effect of the inhibitors on nanoparticle uptake in blood. (**A**) Experimental workflow. DiD-labeled liposomes, DiD-labeled mRNA LNPs, and SPIO NWs were incubated in lepirudin blood, with or without complement inhibitors. Following incubation, the uptake (MFI for DiD-labeled particles and the number of cells retained on the magnetic column for SPIO NWs) was analyzed. (**B** and **C**) Representative UMAP plots of blood leukocytes following incubation with DiD-labeled mRNA LNPs (B) and liposomes (C). Left: Cell populations. Right: DiD uptake heatmap. Neutrophils, monocytes, and B cells are responsible for most of the uptake. (**D**) Gating of leukocytes (Gr, granulocytes; M, monocytes) based on the forward scatter–side scatter (FSC-SSC) plot and then on DiD fluorescence. (**E**) MFI of granulocytes (left graph) and monocytes (right graph) in healthy donors ($N = 5$) and the effect of inhibitors. Iptacopan is effective in some donors, whereas CR2-CR1 is effective in all donors. The percentages of DiD^+ granulocytes and monocytes are in fig. S4. SPIO NWs show high uptake only in donor F66-1, which is inhibited completely by CR2-CR1 and partially by iptacopan (EDTA, 20 mM; CR2-CR1, 10 nM; iptacopan, 20 μM).

types recognize liposomes and mRNA LNPs. After staining leukocytes for phenotypical markers CD14, CD15, CD16, CD11b, CD66b, CD3, CD19, and CD56, we used nonsupervised Uniform Manifold Approximation and Projection for Dimension Reduction (UMAP) combined with manual gating to define cell populations (Fig. 4, B and C and fig S2 for the gating strategy). Mapping of DiD mean fluorescence intensity (MFI) on the UMAP plot revealed that B lymphocytes, neutrophils, eosinophils, and $CD11b^+$ monocytes took up liposomes and LNPs. In contrast, CD11b-negative cells, including T lymphocytes, natural killer (NK) cells, and CD11b-negative monocytes, showed no uptake.

Next, we measured the efficacy of inhibition of the uptake of liposomes, LNPs, and SPIO NWs by granulocytes and monocytes in the blood from five healthy donors using 10 nM CR2-CR1, 20 μM iptacopan, or 10 mM EDTA. For liposomes and mRNA LNPs, the granulocytes were gated on the basis of forward/side scattering (Fig. 4C). Then, MFI of DiD and percentage of DiD^+ cells were determined (Fig. 4D). Because SPIO NWs are nonfluorescent, we determined the uptake as the number of the magnetic granulocytes eluted from magnetic-activated cell sorting (MACS) column (fig. S3). The results revealed that CR2-CR1 caused between 90 and 95% reduction in the DiD MFI of granulocytes and monocytes (Fig. 4E) and a major reduction in the percentage of DiD^+ granulocytes (fig. S4). The effect on the percentage of DiD^+ monocytes was less pronounced, likely due to existence of a secondary, non-inhibitable uptake pathway (fig. S4). Only one donor showed measurable uptake of SPIO NWs, and it was reduced by 95% by CR2-CR1 (Fig. 4E). On the other hand, iptacopan efficacy with liposomes and LNPs was variable and was effective in three of five donors (Fig. 4E). Iptacopan was partially effective with SPIO NWs (~60% reduction in the number of magnetic cells). This result suggests that iptacopan's efficacy is nanoparticle and donor dependent, whereas CR2-CR1 works in all donors and for multiple nanoparticle types.

Iptacopan prevents complement-dependent uptake of bolus-injected SPIO NWs in mice, rats, and dogs

On the basis of the promising efficacy of iptacopan and danicopan in human sera, we measured the IC_{50} for SPIO NWs in sera from BALB/c mice, Sprague-Dawley rats, and various breeds of dogs. In mouse serum, iptacopan demonstrated a single-digit micromolar IC_{50}. In contrast, danicopan exhibited poor inhibition (Fig. 5A). In rat serum, iptacopan displayed a low micromolar IC_{50} and more than 90% inhibition at 100 μM (Fig. 5B). In comparison, danicopan inhibited less than 50% of C3 at 100 μM (Fig. 5B). In dog sera from two breeds, iptacopan showed a low micromolar IC_{50} (Fig. 5C) and significant inhibition at 10 μM across five breeds (Fig. 5D). Danicopan was considerably less effective (Fig. 5D). Previously, we found that CR2-CR1 is highly potent in human and rat sera. Unexpectedly, CR2-CR1 was inactive in dog sera (Fig. 5E), suggesting species-specific inhibition of C3 convertases.

On the basis of the activity of iptacopan in vitro in animal sera, we aimed to test the in vivo inhibition of C3 opsonization and blood immune uptake of SPIO NWs in mice, rats, and dogs. NWs, either alone or premixed with iptacopan, were bolus injected intravenously, and nanoparticles and leukocytes were recovered at various times after injection (Fig. 6A). Female BALB/c mice were injected with NWs (10 mg Fe/kg) alone or in combination with iptacopan intravenously (0.63 mg/kg, premixed with NWs) or with intraperitoneal (IP; 6.34 mg/kg, injected 60 min before SPIO NWs). Flow cytometry (forward scatter versus side scatter of magnetic cells demonstrated significant inhibition of immune uptake by granulocytes at 30 and 60 min postinjection (Fig. 6, B and C). Monocytes and lymphocytes exhibited partial inhibition (Fig. 6B). In addition, intravenous (IV) iptacopan significantly decreased C3 opsonization of NWs retrieved from plasma 5 min after the injection (Fig. 6D).

In Sprague-Dawley rats, a bolus IV injection of iptacopan at two different doses [0.21 mg/kg (low dose) and 0.99 mg/kg (high dose) with SPIO NWs (6.6 mg/kg)] inhibited uptake by blood leukocytes

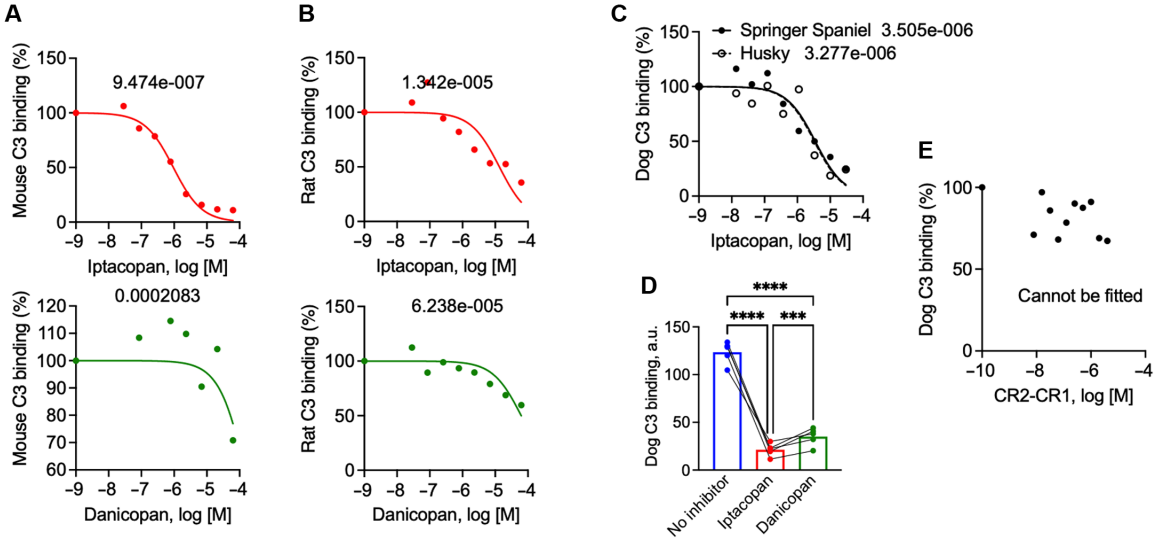

Fig. 5. Inhibition of SPIO NW opsonization with C3 in animal sera in vitro. IC_{50} curves in (**A**) mouse and (**B**) rat sera. Iptacopan maintains its efficacy across species, while danicopan appears to be less effective. (**C**) IC_{50} curves for iptacopan in serum from Springer Spaniel and Husky demonstrate dose-dependent inhibition. (**D**) Inhibition of C3 opsonization in dog sera by 10 μM iptacopan and 10 μM danicopan. Two-way analysis of variance (ANOVA) with multiple comparisons, $N = 5$ breeds, $^{***}P < 0.001$ and $^{****}P < 0.0001$. (**E**) CR2-CR1 is ineffective in dog serum. Repeated twice.

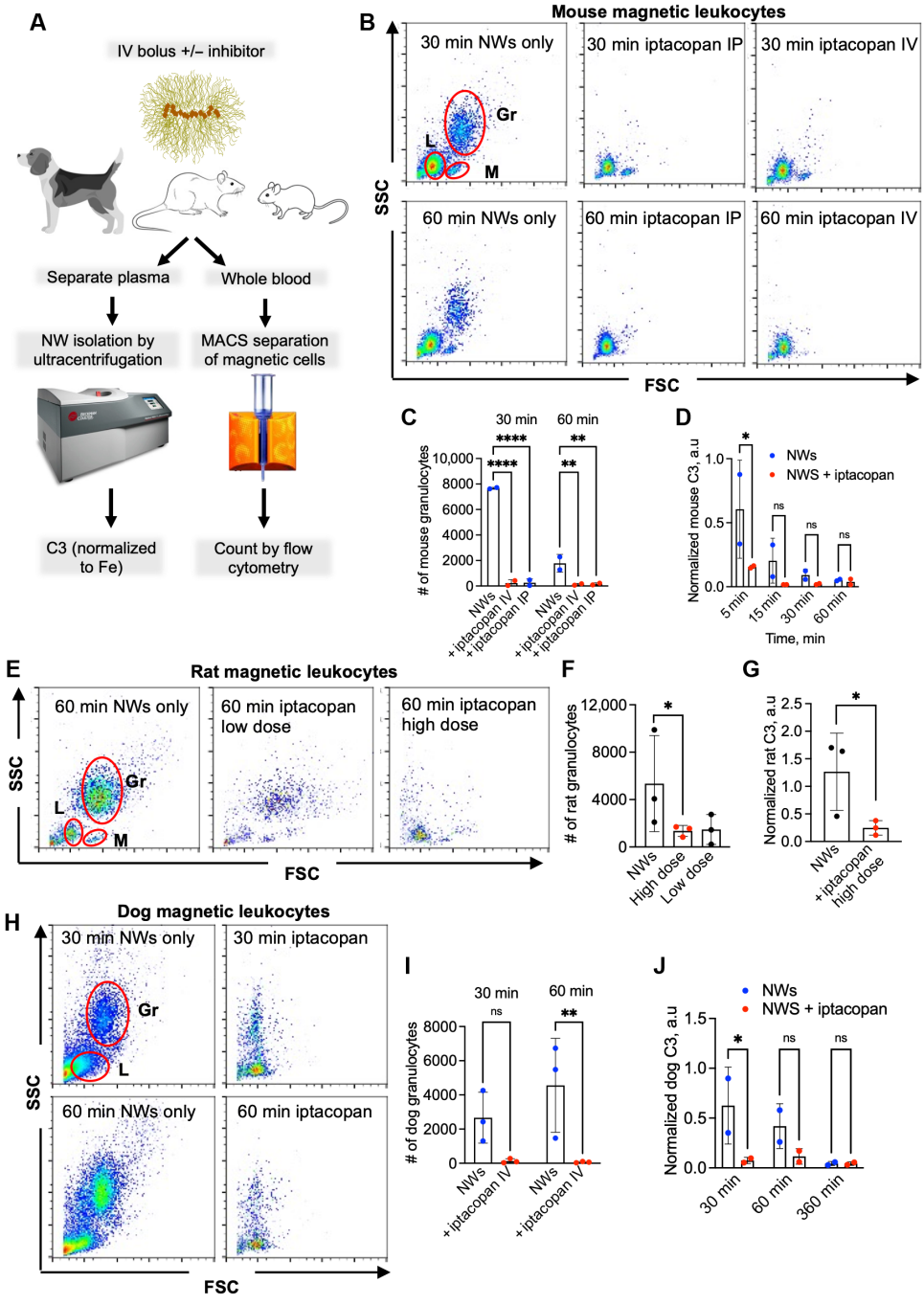

Fig. 6. Inhibition of immune uptake and C3 opsonization by iptacopan in mice, rats, and dogs in vivo. (**A**) Workflow of the experiment. SPIO NWs were injected IV alone or with iptacopan in BALB/c mice, Sprague-Dawley rats, or Beagle dogs. Leukocytes were isolated from blood postinjection using a magnetic column. Magnetically labeled cells were analyzed through FSC-SSC gating to differentiate lymphocytes, monocytes, and granulocytes. NWs were isolated from plasma with ultracentrifugation and normalized to Fe to analyze C3 deposition. (**B** and **C**) Mouse leukocytes' uptake of SPIO NWs 30 and 60 min postinjection. The coadministration of iptacopan completely blocks the uptake by granulocytes. In a separate experiment, iptacopan administered intraperitoneally 30 min before SPIO NWs is equally effective as iptacopan administered IV. (**D**) Inhibition of mouse C3 deposition on SPIO NWs by iptacopan. (**E** and **F**) Rat leukocytes' uptake of SPIO NWs 60 min post-IV injection. Coadministration of high-dose iptacopan significantly blocks SPIO NW uptake by granulocytes. L, lymphocytes; M, monocytes; Gr, granulocytes. (**G**) High-dose iptacopan significantly reduces rat C3 deposition on SPIO NWs. (**H** and **I**) Dog leukocytes' uptake 30 and 60 min postinjection of SPIO NWs. Iptacopan significantly reduces uptake at 30 and 60 min. (**J**) C3 deposition on SPIO NWs indicates significant inhibition by iptacopan at 30 min. Two-way ANOVA with multiple comparisons, $N = 3$ animals per group, $^{*}P < 0.05$, $^{**}P < 0.01$, and $^{****}P < 0.0001$. Bar graphs show means and SD. ns, not significant.

at 60 min postinjection (Fig. 6E), with high-dose iptacopan achieving significant inhibition of granulocytes (Fig. 6F). In addition, high dose of iptacopan blocked more than 90% of rat C3 opsonization of NWs at 60 min postinjection (Fig 6G).

In Beagle dogs, a bolus IV coinjection iptacopan (0.43 mg/kg) with SPIO NWs (6.6 mg/kg) significantly reduced the number of magnetic granulocytes (Fig. 6, H and I). Unlike in mice and rats, we could not accurately define monocytes using forward scatter versus side scatter, thus preventing us from observing the effect of the inhibitor on uptake by monocytes. In addition, iptacopan significantly decreased dog C3 opsonization in the blood at 30 min postinjection (Fig. 6J).

Iptacopan prevents acute reactions associated with bolus-injected SPIO NWs in rats and dogs

Previously, we reported that following a bolus injection of NWs, rats exhibited decreased mobility and lethargy, which was effectively prevented by coinjection with CR2-CR1 (*21*). Rearing behavior (standing on hindlimbs) serves as a quantitative indicator of well-being in non-anesthetized rats (*35*), and we hypothesized that the frequency of rearings could be used to measure the severity of reactions to nanoparticles. As shown in Fig. 7A, NWs significantly decreased the number of rearings by threefold compared to the noninjected control. In contrast, coinjection of either a low or a high dose of iptacopan led to a significant increase in rearings (Fig. 7A). While the involvement of complement is undeniable based on these data, the downstream effector of these responses is not clear. Plasma levels of inflammatory cytokines interleukin-1β and tumor necrosis factor–α were normal after injection of NWs (fig. S5), suggesting that the observed acute reactions are not associated with cytokine release. However, the levels of C5a following the injection of NWs exhibited a brief increase above the background (fig. S6). Coinjection of NWs with the cyclic hexapeptide receptor antagonist of C5a receptor 1 (C5aR1), PMX53 that has activity in rats (*36*, *37*) at either 1 mg/kg IV, or 3 mg/kg IP + 1 mg/kg IV, did not restore the diminished rearing behavior (Fig. 7A). Combined, these data suggest anaphylatoxin-independent mechanisms of the reactions in rats.

In Beagle dogs, the IV bolus SPIO NWs (6.6 mg/kg) resulted in a rapid decrease in both systolic and diastolic pressure (Fig. 7, C and D). Coinjection with iptacopan IV restored systolic and diastolic pressure. The statistical analysis indicated significant differences in both diastolic and systolic pressure between groups, whether compared between groups (Fig. 7, B and C) or normalized to the effect in the same dog before and after the injection (Fig. 7, D and E, and supplementary data).

DISCUSSION

Nanomedicines are prone to hypersensitivity reactions and immune uptake, which present clinical challenges (*1*). Our previous studies described infusion reactions in rats caused by bolus injection of SPIO NWs and highlighted the potential efficacy of CR2-CR1 in reducing

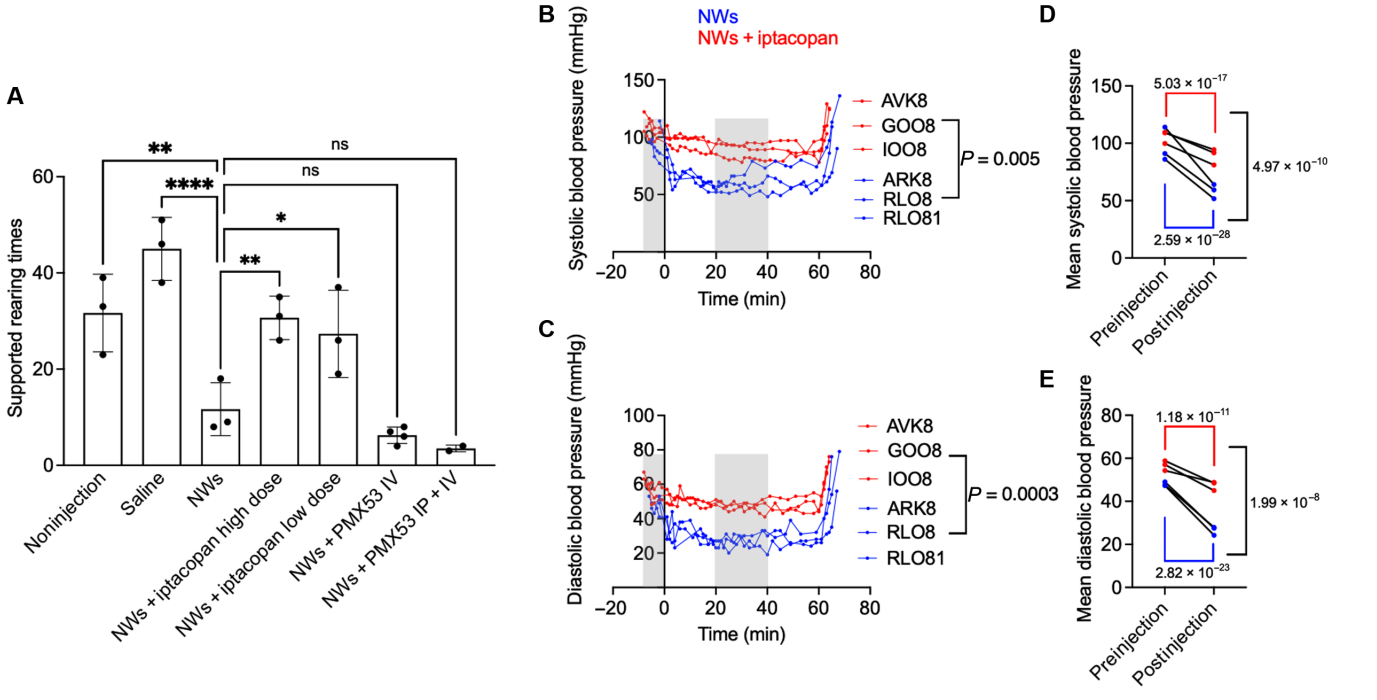

Fig. 7. Iptacopan prevents adverse reactions to bolus-injected SPIO NWs. (**A**) Supported rearing times (during 10 min) serve as an indicator of systemic reactions in rats. Rats injected with NWs exhibit significantly reduced rearing behavior. In contrast, rats coinjected with iptacopan show significantly normalized rearing behavior. Rearing times were not significantly increased by coinjection of NWs with C5R1 antagonist PMX53 (administered either IV or IP + IV). Bar graphs show means and SD. Two-way ANOVA with multiple comparisons, $N = 3$ rats per group, $^{*}P < 0.05$, $^{**}P < 0.01$, and $^{****}P < 0.0001$. (**B** and **C**) Blood pressure measurements in anesthetized Beagle dogs (labels show unique code names for each dog, $N = 3$ per group). Both systolic (B) and diastolic (C) pressures decrease with the induction of anesthesia but start to drop drastically after NW bolus injection (time 0). Coinjection with iptacopan prevents the drop in blood pressure. The *P* values indicate differences between groups. (**D** and **E**) *P* values for the interaction effect [i.e., the difference in nanoparticle-induced changes in systolic blood pressure before and after injection [gray areas in (B) and (C) both within each group and between the control and the inhibitor groups]. Statistical analysis in the Supplementary Materials.

these immune responses (*21*). The current study demonstrates that a recently FDA-approved complement inhibitor, iptacopan, can effectively mitigate complement-associated immune responses and enhance the hemocompatibility of systemically administered SPIO NWs in multiple animal species. Furthermore, we gained robust data on the effectiveness of complement inhibitors in human serum and blood. Despite that, the value of complement inhibitors in improving the hemocompatibility of nanomedicines in humans remains uncertain. Translating findings from animal models to clinical practice is complicated, as the molecular mechanisms underlying mild to severe allergic symptoms differ between cases and are still poorly understood (*4*). Reactogenicity of various nanoparticles has been reported in pigs (*38*), although the contribution of complement in humans has been questioned (*39*). Unexpectedly, we observed a lack of effect of the C5aR1 antagonist PMX53 on the responses induced by SPIO NWs in rats. Anaphylatoxin-independent macrophage activation following uptake may contribute to the reactogenicity (*5*, *39*). Complement inhibitors effectively block uptake by blood neutrophils and monocytes in mice, rats, and dogs. These results highlight the dual role of complement inhibitors in mitigating immune uptake and inflammation, underscoring their therapeutic potential for enhancing the safety and efficacy of nanoparticle-based therapies. At the same time, uptake by resident tissue macrophages such as the hepatic Kupffer cells could be more complex than just complement and may involve additional mechanisms. Therefore, it needs to be investigated within a different scope of work.

While more work needs to be done, our strategy seeks to ultimately expand the use of complement inhibitors in conjunction with existing FDA-approved nanotherapies. This orthogonal approach to preventing opsonization presents a promising opportunity to improve patient safety in nanoparticle-based treatments by using approved drugs instead of the translationally challenging engineering of nanoparticle surfaces (*40*). Furthermore, using complement pathway inhibitors provides an opportunity to identify the key components responsible for nanoparticle-induced immune responses toward nanomedicines and biologics (*41*). That said, determining the ideal clinical trial population—healthy individuals versus patients at risk of nanoparticle-related reactions—presents a significant challenge (*25*). Given the donor-dependent variability of complement activation and uptake of nanoparticles [often determined by levels of anti-PEG antibodies and possibly the levels of complement proteins (*25*, *42*, *43*)], prescreening patients at risk of high complement activation and uptake may serve as an effective strategy to identify persons at "risk" on IRs.

Another question is which pathway inhibitor to choose in combination with nanoparticles. Nanoparticles trigger complement activation in different ways, which is modulated by their curvature and architectural and surface pattern arrangements, including chemical composition, the density and spacing periodicity of surface functional groups, and the conformational state of surface projected macromolecules (*44*–*48*). Thus, complement activation could proceed through any of the three established complement pathways or combinations thereof since these parameters modulate multivalent engagement with and conformational regulation of surface-bound antibodies and complement pattern recognition molecules (*48*). The mechanism by which anti-PEG antibodies activate complement remains unclear, as this and other studies rule out the involvement of the classical pathway via anti-PEG antibodies (*32*, *49*). There is evidence for the activation of the lectin pathway by PEGylated nanoparticles (*50*). Direct deposition of C3(H_2O) on nanoparticle surfaces could also lead to nonproteolytic complement activation (*31*). Furthermore, nonspecific blood proteins also adsorb onto nanoparticle surfaces, and these, in turn, could trigger complement activation (*32*, *51*). Considering diversities in nanoparticle size and surface properties, as well as multifaceted pathways that lead to complement activation, universal approaches are needed to suppress complement activation by existing and forthcoming nanopharmaceuticals. Thus, the availability of regulatory-approved complement inhibitors (*12*) might offer viable, flexible, and stratified approaches to overcoming complement responses to administered nanopharmaceuticals.

In light of the above arguments, pan-inhibitors like CR2-CR1 may be favored, as they prove effective in most subjects. Iptacopan was effective with some particle types, such as SPIO NWs and CLIO NWs, and only in some donors. Further studies involving blood-derived proteome of nanoparticles and complement pathway mapping can shed light on nanoparticle- and subject-dependent differences in the efficacy of iptacopan. Nevertheless, since iptacopan is a clinically approved oral drug, it would be the easiest candidate for clinical investigation. The preclinical advantage of iptacopan is that it inhibits factor B (FB) in multiple animal species, as opposed to human CR2-CR1 and CR1, which are not effective in mice and dogs (*21*, *52*) and may require reengineering for these species. If successful in clinical trials, especially in patients with high levels of complement activation and immune uptake, complement inhibitors could provide a viable method for improving safety and treatment outcomes. However, because of the rapid turnover of complement factors in the liver and other tissues, sustained therapeutic levels require continuous administration, increasing the risk of infections (*53*, *54*)—a concern highlighted by iptacopan's FDA black-box warning. Complement inhibitors coadministered as a bolus with nanoparticles may be safer than chronically administered inhibitors due to their short-acting effect. Future studies should explore the effect of complement inhibitors on the safety and efficacy of nanotherapies.

In summary, this study demonstrates that complement inhibitors can enhance the hemocompatibility and immunocompatibility of nanoparticles in multiple animal species and human donors. While progress has been made, translational challenges remain, particularly in predicting and managing human hypersensitivity reactions. By addressing these challenges through rigorous mechanistic studies and targeted clinical trials, complement inhibitors hold promise for enhancing the safety and efficacy of nanoparticle-based therapies in clinical settings.

MATERIALS AND METHODS

Iron oxide nanoparticles and liposomes

Chemicals used for iron oxide nanoparticle synthesis, including iron salts, epichlorohydrin, and ammonia, were purchased from Sigma-Aldrich (Saint Louis, MO, USA). Pharmaceutical grade dextran (20-kDa molecular weight, T-20) was from Pharmacosmos (Holbæk, Denmark). NWs for animal injections were made aseptically, and an endotoxin level below 2 EU/ml was confirmed using the Pierce Chromogenic Endotoxin Quant Kit (Thermo Fisher Scientific). Liposomal lipids [hydrogenated soy phosphatidylcholine (HSPC), PEG_{2000}–distearoyl phosphatidylethanolamine (DSPE-PEG_{2000}), and cholesterol] were from Avanti Polar Lipids (Alabaster, AL, USA). SPIO NWs and cross-linked CLIO NWs were synthesized following a previously reported method (*55*). PLD and Onivyde were sourced as sterile vials from the University of Colorado Cancer Center infusion pharmacy.

For PEGylated liposomes, HSPC/cholesterol/DSPE-PEG_{2000} mix in chloroform (56.6/38/5 molar ratio) with the addition of 0.2% DiD in chloroform was dried under nitrogen, and small unilamellar vesicles were prepared by the dehydration-rehydration method as described before (*56*). Liposomes were extruded by a syringe extruder (Avestin, Ottawa, Canada) through Whatman Nuclepore Track-Etched Membranes (100-nm pore size, 21 times; 57°C). Nanoparticle size distribution (intensity-weighted diameter) was measured using a Malvern Zetasizer Nano ZS instrument.

LNP formulation

mRNA-containing LNPs were formulated using in vitro–transcribed enhanced green fluorescent protein mRNA containing CleanCap Reagent AG (TriLink Biotechnologies, #N-7113), N^1-methylpseudouridine-5′-triphosphate (TriLink Biotechnologies, #N-1081), optimized 5′ and 3′ untranslated region sequences, and an enzymatically added polyA tail [*Escherichia coli* polyA polymerase; New England Biolabs (NEB), #M0276]. The lipid mix contained DLin-MC3-DMA (Cayman Chemical, #34364), 1,2-distearoyl-*sn*-glycero-3-phosphocholine (Avanti Polar Lipids, #850365P), cholesterol (MilliporeSigma, #C8667), and 1,2-dimyristoyl-rac-glycero-3-methoxypolyethylene glycol-$_{2000}$ (Avanti Polar Lipids, #880151P), in a 50:10:38.5:1.5 molar ratio. DiD was added to the lipid mix at 0.1%. LNPs were produced by microfluidic mixing of the RNA solution in 0.1 M sodium acetate buffer (pH 4.0), with the lipid mixture in ethanol using a NanoAssemblr Spark (Precision Nanosystems) at a flow rate ratio of 2:1 (RNA:lipid) and a N=negative/positive charge (N/P) ratio of 4 (amine:phosphate). LNPs were diluted in phosphate-buffered saline (PBS) (pH 7.4) (Corning, #21-040-CV) and dialyzed against 1× PBS using a 3.5 K molecular weight cutoff mini dialysis device (Thermo Fisher Scientific, #88400) for 2 hours at 4°C with one buffer change. The encapsulation efficiency and the concentration of encapsulated mRNA were determined using a Quant-iT RiboGreen RNA assay (Thermo Fisher Scientific, #R11490). Size distribution (intensity-weighted diameter) was measured using Zetasizer Nano ZS.

Complement assays

For serum measurements of C3 deposition and C5a release, whole blood (3 to 20 ml) was collected in a Vacutainer Z without anticoagulant. For nanoparticle uptake, lepirudin-anticoagulated blood (3 to 5 ml, 10 μg lepirudin/ml blood) was collected. Blood was obtained at the University of Colorado Blood Donor Center (human subjects exemption: no Institutional Review Board approval was required as part of routine blood donation). Only age and sex were made available to the investigators. Blood was not collected if donors were febrile, unwell, or taking systemic antibiotics. Collection and screening of plasma with variable titers of anti-PEG antibodies were done according to the University of Colorado Hospital Emergency Department under Colorado Multiple Institutional Review Board protocol 17-1642, as described in the previous publication (*25*).

C3 deposition was measured using a previously described and validated immuno-dot blot protocol (*22*) using corresponding species-specific anti-C3 antibodies (*57*). Iptacopan and danicopan (catalog nos. 37291 and 32737, respectively, Cayman Chemical, Ann Arbor, MI) were stored as 10 to 100 mM stocks in dimethyl sulfoxide. CR2-CR1 was prepared in the laboratory of S.A.T., Medical University of South Carolina. Briefly, nanoparticles in PBS were mixed with serum or plasma (final concentration of serum, 75%; 0.25 mg/ml of Fe for SPIO NWs and CLIO NWs and 0.25 mg/ml of doxorubicin or irinotecan for PLD and Onivyde), with or without EDTA (final concentration, 10 mM) or varying concentrations of complement inhibitors and incubated at 37°C for 30 min. The volume of the inhibitors was 2 μl. The nanoparticles were washed three times with PBS at 450,000*g* and 4°C using a Beckman Optima Max-XP ultracentrifuge equipped with a TLA-100.3 rotor. Pellets were resuspended in PBS to a final concentration of 0.1 mg Fe or drug/milliliter, and 2 μl was applied in three to four replicates onto a 0.45-μm nitrocellulose membrane. Membranes were probed using polyclonal goat anti-human C3 antibody (MP Biomedicals), mouse anti-human C3d neoepitope antibody (A250, Quidel, San Diego, CA), or polyclonal rabbit anti-human C4d antibody [provided by N.K.B., University of Colorado and described elsewhere (*58*)] and corresponding IR800-labeled secondary antibodies and scanned using an Odyssey infrared imager (LI-COR Biosciences), after which dot intensities were analyzed with Fiji (ImageJ2 v2.9.0). Data were normalized to the "no inhibitor" control and fitted to a normalized inhibition curve using Prism v. 10 software to calculate IC_{50} values. Human C5a levels following incubation of serum with nanoparticles (0.25 mg/ml Fe/drug or 0.025 mg/ml of mRNA) for 30 min at 37°C were measured using a Human Complement Component C5a DuoSet enzyme-linked immunosorbent assay (ELISA) kit (DY2037, BioTechne) according to the manufacturer's protocol (1:100 to 1:400 plasma dilution). Plates were read with a SpectraMax Gemini EM Microplate Reader, and data were analyzed using SoftMax Pro 5.2 software (Molecular Devices).

For in vivo complement C3 deposition, NWs were recovered from plasma by ultracentrifugation. Iron concentration was measured using a ferrozine assay and normalized to 0.02 mg/ml for all time points before application onto the membrane. C3 protein detection was conducted using primary anti-mouse, anti-rat, and anti-dog C3 antibodies. Rat C5a levels in plasma recovered from rats before and after injection of SPIO NWs were measured according to the manufacturer's instructions using a rat C5a ELISA kit (MBS160277) from Mybiosource.com.

Blood uptake

Fresh lepirudin-anticoagulated human blood was used to analyze the uptake. Briefly, 200 μl of blood and 10 μl of DiD-labeled liposomes (final concentration, 1.65 μM DiD) or 2 μl of LNPs (final concentration, 1 μg/ml mRNA) or 10 μl of SPIO NWs (final concentration, 50 μg/ml Fe) were mixed and incubated at 37°C with gentle rotation. After 1-hour incubation, cells were washed with PBS, RBCs were lysed, and blood was fixed with BD Lyse/Fix Reagent 558049 from BD Biosciences. Cells were submitted along with a control (no nanoparticles) to the Flow Cytometry Core at the University of Colorado Cancer Center. Cells were stained for the markers described in table S2. All antibodies were from BioLegend (San Diego, CA), except anti-CD14, CD16, and CD66b, which were from BD Biosciences. NK cells (CD56) and T cells (CD3) were acquired in the same dump PerCP-Cy5.5 channel, and NK cells were then identified on the basis of $CD16^+$ expression. The data were acquired with a Cytek Aurora flow cytometer and analyzed with FlowJo v10.10.0. The Flow AI plugin was applied to clean the data, and dimensionality reduction analysis was performed using the UMAP R plugin (FlowJo Exchange). Cell populations were gated manually and dragged on the UMAP plot. The gating strategy is in the Supplementary Materials,

and information on spectral unmixing and instrument calibration with beads is available upon request.

To assess the efficacy of the inhibitors, the experiments were conducted in a manner similar to the above with the addition of inhibitors to the blood. For liposome and LNP analysis, the blood was lysed. Cells were analyzed for uptake using a Guava EasyCyte HT flow cytometer (Cytek Biosciences, Fremont, CA, USA) and using FlowJo software v. 10. Forward scatter–side scatter (FSC-SSC) plots were used to eliminate debris and identify leukocyte populations, including granulocytes, lymphocytes, and monocytes. Each population was assessed for DiD fluorescence. For SPIO NW uptake, blood was diluted in 1% (w/v) bovine serum albumin (BSA) in PBS and passed through a magnetic Mini MS column mounted on an OctoMACS separator (both from Miltenyi Biotec). The column was washed with 1 ml of 1% BSA/PBS, and the magnetic cell fractions were eluted, centrifuged at 500*g* for 4 min, resuspended in 500 μl of 1% BSA/PBS, and run on a Guava EasyCyte HT flow cytometer. Data were analyzed with FlowJo v. 10. FSC-SSC plots were used to exclude debris and identify leukocyte populations, including neutrophils, lymphocytes, and monocytes, and calculate MFI. For SPIO NW uptake, the counts of eluted magnetic cells (acquired for 30 s) were compared between control and inhibitor samples. For in vivo uptake analysis, EDTA-anticoagulated blood was collected from mice, rats, and dogs injected with SPIO NWs alone or in combination with iptacopan. Blood samples (100 μl) were centrifuged at 500g for 5 min to separate the plasma and then processed using the magnetic column as previously described above.

Animal injections

The animal experiments were conducted under the University of Colorado Institutional Animal Care and Use Committee (IACUC) protocol 103913(11) for mice and rats and HQR, LLC IACUC protocol 209.001 for dogs. Mice received IV injections of SPIO NWs (10 mg/kg) with or without iptacopan (0.016 mg/kg). Sprague-Dawley rats (250 to 330 g) received SPIO NWs (6.7 mg/kg) with or without iptacopan (0.211 mg/kg). Beagle dogs (7 to 12.5 kg) received SPIO NWs (6.7 mg/kg) with or without iptacopan (0.4285 mg/kg). The injected dose contained less than 2 EU/kg endotoxin. Blood was collected via the periorbital plexus (mice), tail vein (rats), or jugular vein (dogs) using EDTA as an anticoagulant.

To measure adverse reactions in rats, Sprague-Dawley rats (females; 250 to 330 g) were restrained in rodent restraining bags and intravenously injected with saline, SPIO NWs, or SPIO NWs premixed with iptacopan or C5aR1 antagonist PMX53. In some experiments, rats were preinjected IP with PMX53, followed by SPIO NWs premixed with PMX53 IV. Five minutes postinjection of NWs, rats were released into individual cages with fresh bedding and dim lighting, and rat movements were recorded using a camera positioned above the cage. Recordings were performed at the same time of the day to minimize variability in the behavior. Activity levels were assessed by counting cage-supported rearings during 10 min in the cage.

Canine experiments were performed at the High Quality Research (Fort Collins, CO, USA). Six female beagle dogs (7 to 12.5 kg) were randomized into two groups ($n = 3$ per group). Before injection, the dogs were anesthetized and placed on operating tables for baseline monitoring of physiological parameters, including pulse rate, blood pressure (diastolic and systolic), heart rate, and body temperature. The dogs were intravenously administered with SPIO NWs (6.6 mg/kg) with or without iptacopan (0.4285 mg/kg), and parameters were continuously recorded for 1 hour postinjection. Following recovery from anesthesia, the dogs were checked by a veterinarian at 3, 6, and 24 hours postinjection for alertness and overall well-being. Behavioral changes indicative of discomfort were noted. Observations were conducted in a controlled environment to ensure consistency across conditions. The effect of iptacopan in dogs was analyzed using two statistical models. In the first analysis, values recorded between 20 and 40 min after injection were included, treating multiple values from the same dog as repeated measures. No time trend or dependency was incorporated into the model. In the second analysis, values recorded before injection (time, <0) were treated as "pretreatment" values, and values recorded between 20 and 40 min after injection were considered "posttreatment" values. This analysis used a linear mixed model with fixed effects for treatment and time points (pre- or posttreatment) and a random effect for the dog.

Supplementary Materials

This PDF file includes:

Figs. S1 to S6
Tables S1 and S2
Statistical analysis for Fig. 7

REFERENCES AND NOTES

1. J. Szebeni, D. Simberg, A. Gonzalez-Fernandez, Y. Barenholz, M. A. Dobrovolskaia, Roadmap and strategy for overcoming infusion reactions to nanomedicines. *Nat. Nanotechnol.* **13**, 1100–1108 (2018).
2. D. Ricklin, G. Hajishengallis, K. Yang, J. D. Lambris, Complement: A key system for immune surveillance and homeostasis. *Nat. Immunol.* **11**, 785–797 (2010).
3. S. M. Moghimi, J. Szebeni, Stealth liposomes and long circulating nanoparticles: Critical issues in pharmacokinetics, opsonization and protein-binding properties. *Prog. Lipid Res.* **42**, 463–478 (2003).
4. S. M. Moghimi, H. B. Haroon, A. Yaghmur, A. C. Hunter, E. Papini, Z. S. Farhangrazi, D. Simberg, P. N. Trohopoulos, Perspectives on complement and phagocytic cell responses to nanoparticles: From fundamentals to adverse reactions. *J. Control. Release* **356**, 115–129 (2023).
5. D. Acharya, X. R. L. Li, R. E. Heineman, R. E. Harrison, Complement receptor-mediated phagocytosis induces proinflammatory cytokine production in murine macrophages. *Front. Immunol.* **10**, 3049 (2019).
6. R. Schmouder, N. Kaetterer, K. Kulmatycki, P. K. Nidamarthy, A phase 1 study to evaluate the pharmacokinetics of single high doses of iptacopan. *Blood* **142**, 2723–2723 (2023).
7. Y. X. Wang, J. M. Idee, A comprehensive literatures update of clinical researches of superparamagnetic resonance iron oxide nanoparticles for magnetic resonance imaging. *Quant. Imaging Med. Surg.* **7**, 88–122 (2017).
8. T. J. Povsic, J. P. Vavalle, L. H. Aberle, J. D. Kasprzak, M. G. Cohen, R. Mehran, C. Bode, C. E. Buller, G. Montalescot, J. H. Cornel, A. Rynkiewicz, M. E. Ring, U. Zeymer, M. Natarajan, N. Delarche, S. L. Zelenkofske, R. C. Becker, J. H. Alexander, RADAR Investigators, A phase 2, randomized, partially blinded, active-controlled study assessing the efficacy and safety of variable anticoagulation reversal using the REG1 system in patients with acute coronary syndromes: Results of the RADAR trial. *Eur. Heart J.* **34**, 2481–2489 (2013).
9. L. H. Calabrese, A. Kavanaugh, A. E. Yeo, P. E. Lipsky, Frequency, distribution and immunologic nature of infusion reactions in subjects receiving pegloticase for chronic refractory gout. *Arthritis Res. Ther.* **19**, 191 (2017).
10. E. D. Weinhandl, D. T. Gilbertson, A. J. Collins, R. N. Foley, Relative safety of peginesatide and epoetin alfa. *Pharmacoepidemiol. Drug Saf.* **23**, 1003–1011 (2014).
11. D. C. Mastellos, D. Ricklin, J. D. Lambris, Clinical promise of next-generation complement therapeutics. *Nat. Rev. Drug Discov.* **18**, 707–729 (2019).
12. E. E. West, T. Woodruff, V. Fremeaux-Bacchi, C. Kemper, Complement in human disease: Approved and up-and-coming therapeutics. *Lancet* **403**, 392–405 (2024).
13. A. Schubart, S. Flohr, T. Junt, J. Eder, Low-molecular weight inhibitors of the alternative complement pathway. *Immunol. Rev.* **313**, 339–357 (2023).
14. M. Reid, B. A. Fedutes Henderson, Sutimlimab for cold agglutinin disease. *J. Adv. Pract. Oncol.* **15**, 389–395 (2024).
15. C. Lamers, X. Xue, M. Smiesko, H. van Son, B. Wagner, N. Berger, G. Sfyroera, P. Gros, J. D. Lambris, D. Ricklin, Insight into mode-of-action and structural determinants of the compstatin family of clinical complement inhibitors. *Nat. Commun.* **13**, 5519 (2022).

16. C. Parker, Eculizumab for paroxysmal nocturnal haemoglobinuria. *Lancet* **373**, 759–767 (2009).
17. M. Harigai, H. Takada, Avacopan, a selective C5a receptor antagonist, for anti-neutrophil cytoplasmic antibody-associated vasculitis. *Mod. Rheumatol.* **32**, 475–483 (2022).
18. M. Fridkis-Hareli, M. Storek, E. Or, R. Altman, S. Katti, F. Sun, T. Peng, J. Hunter, K. Johnson, Y. Wang, A. S. Lundberg, G. Mehta, N. K. Banda, V. Michael Holers, The human complement receptor type 2 (CR2)/CR1 fusion protein TT32, a novel targeted inhibitor of the classical and alternative pathway C3 convertases, prevents arthritis in active immunization and passive transfer mouse models. *Mol. Immunol.* **105**, 150–164 (2019).
19. M. Noris, G. Remuzzi, Overview of complement activation and regulation. *Semin. Nephrol.* **33**, 479–492 (2013).
20. M. Krych, L. Clemenza, D. Howdeshell, R. Hauhart, D. Hourcade, J. P. Atkinson, Analysis of the functional domains of complement receptor-type-1 (C3b/C4b receptor, Cd35) by substitution mutagenesis. *J. Biol. Chem.* **269**, 13273–13278 (1994).
21. Y. Li, S. Jacques, H. Gaikwad, G. Wang, N. K. Banda, V. M. Holers, R. I. Scheinman, S. Tomlinson, S. M. Moghimi, D. Simberg, Inhibition of acute complement responses towards bolus-injected nanoparticles using targeted short-circulating regulatory proteins. *Nat. Nanotechnol.* **19**, 246–254 (2024).
22. Y. Li, A. Monte, L. Dylla, S. M. Moghimi, D. Simberg, Validation of dot blot immunoassay for measurement of complement opsonization of nanoparticles. *J. Immunol. Methods* **528**, 113668 (2024).
23. I. Urits, D. Swanson, M. C. Swett, A. Patel, K. Berardino, A. Amgalan, A. A. Berger, H. Kassem, A. D. Kaye, O. Viswanath, A review of patisiran (ONPATTRO®) for the treatment of polyneuropathy in people with hereditary transthyretin amyloidosis. *Neurol. Ther.* **9**, 301–315 (2020).
24. J. Szebeni, G. Storm, J. Y. Ljubimova, M. Castells, E. J. Phillips, K. Turjeman, Y. Barenholz, D. J. A. Crommelin, M. A. Dobrovolskaia, Applying lessons learned from nanomedicines to understand rare hypersensitivity reactions to mRNA-based SARS-CoV-2 vaccines. *Nat. Nanotechnol.* **17**, 337–346 (2022).
25. Y. Li, L. Saba, R. I. Scheinman, N. K. Banda, M. Holers, A. Monte, L. Dylla, S. M. Moghimi, D. Simberg, Nanoparticle-binding immunoglobulins predict variable complement responses in healthy and diseased cohorts. *ACS Nano* **18**, 28649–28658 (2024).
26. C. L. Harris, M. Heurich, S. Rodriguez de Cordoba, B. P. Morgan, The complotype: Dictating risk for inflammation and infection. *Trends Immunol.* **33**, 513–521 (2012).
27. A. Chanan-Khan, J. Szebeni, S. Savay, L. Liebes, N. M. Rafique, C. R. Alving, F. M. Muggia, Complement activation following first exposure to pegylated liposomal doxorubicin (Doxil): Possible role in hypersensitivity reactions. *Ann. Oncol.* **14**, 1430–1437 (2003).
28. M. E. Senti, C. A. de Jongh, K. Dijkxhoorn, J. J. F. Verhoef, J. Szebeni, G. Storm, C. E. Hack, R. M. Schiffelers, M. H. Fens, P. Boross, Anti-PEG antibodies compromise the integrity of PEGylated lipid-based nanoparticles via complement. *J. Control. Release* **341**, 475–486 (2022).
29. E. Chen, B. M. Chen, Y. C. Su, Y. C. Chang, T. L. Cheng, Y. Barenholz, S. R. Roffler, Premature drug release from polyethylene glycol (PEG)-coated liposomal doxorubicin via formation of the membrane attack complex. *ACS Nano* **14**, 7808–7822 (2020).
30. F. Bexborn, P. O. Andersson, H. Chen, B. Nilsson, K. N. Ekdahl, The tick-over theory revisited: Formation and regulation of the soluble alternative complement C3 convertase ($C3(H_2O)Bb$). *Mol. Immunol.* **45**, 2370–2379 (2008).
31. Y. Klapper, O. A. Hamad, Y. Teramura, G. Leneweit, G. U. Nienhaus, D. Ricklin, J. D. Lambris, K. N. Ekdahl, B. Nilsson, Mediation of a non-proteolytic activation of complement component C3 by phospholipid vesicles. *Biomaterials* **35**, 3688–3696 (2014).
32. V. P. Vu, G. B. Gifford, F. Chen, H. Benasutti, G. Wang, E. V. Groman, R. Scheinman, L. Saba, S. M. Moghimi, D. Simberg, Immunoglobulin deposition on biomolecule corona determines complement opsonization efficiency of preclinical and clinical nanoparticles. *Nat. Nanotechnol.* **14**, 260–268 (2019).
33. Y. Li, S. Moein Moghimi, D. Simberg, Complement-dependent uptake of nanoparticles by blood phagocytes: Brief overview and perspective. *Curr. Opin. Biotechnol.* **85**, 103044 (2024).
34. G. Gifford, V. P. Vu, N. K. Banda, V. M. Holers, G. Wang, E. V. Groman, D. Backos, R. Scheinman, S. M. Moghimi, D. Simberg, Complement therapeutics meets nanomedicine: Overcoming human complement activation and leukocyte uptake of nanomedicines with soluble domains of CD55. *J. Control. Release* **302**, 181–189 (2019).
35. O. Sturman, P. L. Germain, J. Bohacek, Exploratory rearing: A context- and stress-sensitive behavior recorded in the open-field test. *Stress* **21**, 443–452 (2018).
36. Y. Shi, Y. Jin, X. Li, C. Chen, Z. Zhang, X. Liu, Y. Deng, X. Fan, C. Wang, C5aR1 mediates the progression of inflammatory responses in the brain of rats in the early stage after ischemia and reperfusion. *ACS Chem. Neurosci.* **12**, 3994–4006 (2021).
37. T. Breivik, Y. Gundersen, P. Gjermo, S. M. Taylor, T. M. Woodruff, P. K. Opstad, Oral treatment with complement factor C5a receptor (CD88) antagonists inhibits experimental periodontitis in rats. *J. Periodontal Res.* **46**, 643–647 (2011).
38. J. Szebeni, J. L. Fontana, N. M. Wassef, P. D. Mongan, D. S. Morse, D. E. Dobbins, G. L. Stahl, R. Bunger, C. R. Alving, Hemodynamic changes induced by liposomes and liposome-encapsulated hemoglobin in pigs: A model for pseudoallergic cardiopulmonary reactions to liposomes. Role of complement and inhibition by soluble CR1 and anti-C5a antibody. *Circulation* **99**, 2302–2309 (1999).
39. P. P. Wibroe, A. C. Anselmo, P. H. Nilsson, A. Sarode, V. Gupta, R. Urbanics, J. Szebeni, A. C. Hunter, S. Mitragotri, T. E. Mollnes, S. M. Moghimi, Bypassing adverse injection reactions to nanoparticles through shape modification and attachment to erythrocytes. *Nat. Nanotechnol.* **12**, 589–594 (2017).
40. J. I. Hare, T. Lammers, M. B. Ashford, S. Puri, G. Storm, S. T. Barry, Challenges and strategies in anti-cancer nanomedicine development: An industry perspective. *Adv. Drug Deliv. Rev.* **108**, 25–38 (2017).
41. E. C. W. de Boer, A. G. van Mourik, I. Jongerius, Therapeutic lessons to be learned from the role of complement regulators as double-edged sword in health and disease. *Front. Immunol.* **11**, 578069 (2020).
42. Y. Ju, H. G. Kelly, L. F. Dagley, A. Reynaldi, T. E. Schlub, S. K. Spall, C. A. Bell, J. Cui, A. J. Mitchell, Z. Lin, A. K. Wheatley, K. J. Thurecht, M. P. Davenport, A. I. Webb, F. Caruso, S. J. Kent, Person-specific biomolecular coronas modulate nanoparticle interactions with immune cells in human blood. *ACS Nano* **14**, 15723–15737 (2020).
43. Y. Ju, S. Li, A. E. Q. Tan, E. H. Pilkington, P. T. Brannon, M. Plebanski, J. Cui, F. Caruso, K. J. Thurecht, C. Tam, S. J. Kent, Patient-specific nanoparticle targeting in human leukemia blood. *ACS Nano* **18**, 29021–29035 (2024).
44. J. B. Coty, E. Eleamen Oliveira, C. Vauthier, Tuning complement activation and pathway through controlled molecular architecture of dextran chains in nanoparticle corona. *Int. J. Pharm.* **532**, 769–778 (2017).
45. Q. H. Quach, J. C. Y. Kah, Correction: Complement activation by gold nanoparticles passivated with polyelectrolyte ligands. *RSC Adv.* **8**, 8247 (2018).
46. M. B. Pedersen, X. Zhou, E. K. Larsen, U. S. Sorensen, J. Kjems, J. V. Nygaard, J. R. Nyengaard, R. L. Meyer, T. Boesen, T. Vorup-Jensen, Curvature of synthetic and natural surfaces is an important target feature in classical pathway complement activation. *J. Immunol.* **184**, 1931–1945 (2010).
47. L. P. Wu, M. Ficker, J. B. Christensen, D. Simberg, P. N. Trohopoulos, S. M. Moghimi, Dendrimer end-terminal motif-dependent evasion of human complement and complement activation through IgM hitchhiking. *Nat. Commun.* **12**, 4858 (2021).
48. H. B. Haroon, E. Dhillon, Z. S. Farhangrazi, P. N. Trohopoulos, D. Simberg, S. M. Moghimi, Activation of the complement system by nanoparticles and strategies for complement inhibition. *Eur. J. Pharm. Biopharm.* **193**, 227–240 (2023).
49. B. M. Chen, E. Chen, Y. C. Lin, T. T. M. Tran, K. Turjeman, S. H. Yang, T. L. Cheng, Y. Barenholz, S. R. Roffler, Liposomes with low levels of grafted poly(ethylene glycol) remain susceptible to destabilization by anti-poly(ethylene glycol) antibodies. *ACS Nano* **18**, 22122–22138 (2024).
50. M. Pannuzzo, S. Esposito, L. P. Wu, J. Key, S. Aryal, C. Celia, L. di Marzio, S. M. Moghimi, P. Decuzzi, Overcoming nanoparticle-mediated complement activation by surface PEG pairing. *Nano Lett.* **20**, 4312–4321 (2020).
51. F. Chen, G. Wang, J. I. Griffin, B. Brenneman, N. K. Banda, V. M. Holers, D. S. Backos, L. Wu, S. M. Moghimi, D. Simberg, Complement proteins bind to nanoparticle protein corona and undergo dynamic exchange in vivo. *Nat. Nanotechnol.* **12**, 387–393 (2017).
52. M. P. Hardy, T. Rowe, S. Wymann, Soluble Complement Receptor 1 Therapeutics. *J. Immunol. Sci.* **6**, 1–17 (2022).
53. E. Benamu, J. G. Montoya, Infections associated with the use of eculizumab: Recommendations for prevention and prophylaxis. *Curr. Opin. Infect. Dis.* **29**, 319–329 (2016).
54. S. R. Barnum, Therapeutic inhibition of complement: Well worth the risk. *Trends Pharmacol. Sci.* **38**, 503–505 (2017).
55. G. Wang, N. J. Serkova, E. V. Groman, R. I. Scheinman, D. Simberg, Feraheme (ferumoxytol) is recognized by proinflammatory and anti-inflammatory macrophages via scavenger receptor type AI/II. *Mol. Pharm.* **16**, 4274–4281 (2019).
56. G. Wang, M. Zannikou, L. Lofchy, Y. Li, H. Gaikwad, I. V. Balyasnikova, D. Simberg, Liposomal extravasation and accumulation in tumors as studied by fluorescence microscopy and imaging depend on the fluorescent label. *ACS Nano* **15**, 11880–11890 (2021).
57. Y. Li, G. Wang, L. Griffin, N. K. Banda, L. M. Saba, E. V. Groman, R. Scheinman, S. M. Moghimi, D. Simberg, Complement opsonization of nanoparticles: Differences between humans and preclinical species. *J. Control. Release* **338**, 548–556 (2021).
58. G. A. Böhmig, H. Regele, M. Exner, V. Derhartunian, J. Kletzmayr, M. D. Säemann, W. H. Hörl, W. Druml, B. Watschinger, C4d-positive acute humoral renal allograft rejection: Effective treatment by immunoadsorption. *J. Am. Soc. Nephrol.* **12**, 2482–2489 (2001).

Acknowledgments: We gratefully acknowledge the assistance of the University of Colorado Anschutz Medical Campus NeuroTechnology Center's Animal Behavior and In Vivo Neurophysiology Core in the planning and analysis of these experiments. We thank the Human Immune Monitoring Shared Resource (RRID:SCR_021985) within the University of Colorado Cancer Center (NIH P30CA046934) for the expert assistance in flow panel development and analysis of leukocyte uptake. **Funding:** The study was supported by the NIH grants: R01CA194058 and R01AI154959 to D.S., R01AG071467 to J.H., P30CA046934 to the University of Colorado Cancer Center, and 1R35GM152157-01 to A.M. Also, we acknowledge

the support by the RNA Bioscience Initiative of the University of Colorado to J.H. S.M.M. acknowledges support by the European Union's Horizon 2020 program funded under H2020-EU.1.3.–Excellent Science–Marie Skłodowska-Curie Actions, grant agreement ID 956544 (DIRNANO: Directing the Immune Response through Designed Nanomaterials). **Author contributions:** Conceptualization: R.I.S., A.M., S.M.M, V.M.H., and D.S. Data curation: L.S., A.M., and D.S. Formal analysis: Y.L., L.S., and D.S. Funding acquisition: J.H., N.K.B., A.M., S.M.M., and D.S. Investigation: Y.L., S.J., M.N., N.K.B., V.M.H., E.L., A.M., N.B., and D.S. Methodology: Y.L., N.K.B., V.M.H., L.S., E.L., J.H., N.B., S.M.M., A.M., and D.S. Project administration: V.M.H. and D.S. Software: L.S. Resources: H.G., M.N., N.K.B., S.A.T., A.M., E.L., J.H., and N.B. Supervision: Y.L., R.I.S., A.M., and D.S. Validation: Y.L., S.J., M.N., N.K.B., and D.S. Visualization: Y.L., S.J., M.N., L.S., and D.S. Writing—original draft: Y.L., S.J., and D.S. Writing—review and editing: N.K.B., V.M.H., S.A.T., L.S., J.H., W.M.Z., R.I.S., A.M., S.M.M., and D.S. **Competing interests:** W.M.Z. is the inventor of the world patent: "Anti-C7 antibody or antibody fragment" related to this work filed by Cardiff University (WO/2021/032860, filed 20 August 2020, published 25 February 2021). The authors declare that they have no other competing interests. **Data and materials availability:** All data needed to evaluate the conclusions in the paper are present in the paper and/or the Supplementary Materials

Submitted 21 January 2025
Accepted 14 May 2025
Published 9 July 2025
10.1126/sciadv.adw1731